Nano Energy 59 (2019) 773–783

Contents lists available at ScienceDirect

Nano Energy

journal homepage: www.elsevier.com/locate/nanoen

Full paper

Flexible artificial synesthesia electronics with sound-synchronized electroluminescence

Jong Sung Kim[a,1], Sung Hwan Cho[a,1], Kang Lib Kim[a], Gwangmook Kim[a], Seung Won Lee[a], Eui Hyuk Kim[a], Beomjin Jeong[a], Ihn Hwang[a], Hyowon Han[a], Wooyoung Shim[a], Tae-Woo Lee[b], Cheolmin Park[a,*]

[a] Department of Materials Science and Engineering, Yonsei University, 50-Yonsei-ro, Seoul, 120-749, Republic of Korea
[b] Department of Materials Science and Engineering, Seoul National University, Gwanak-ro, Gwanak-gu, Seoul, 08826, Republic of Korea

ARTICLE INFO

Keywords:
Sound-synchronized electroluminescence
Artificial synesthesia
Human-sound interaction
Piezoelectric composite film
Field-induced electroluminescence

ABSTRACT

Visualization of human senses has been of great interest for developing an emerging interactive display that can artificially stimulate synesthesia with numerous unprecedented applications. Especially, visualization of various daily sound and music, which are much more complicated than human touch, in a form of flexible thin film devices can be a great challenge. We present flexible artificial synesthesia electronics that visualize continuous and complicated sounds. The electronic device is made of a thin composite film of a piezoelectric polymer for sound generation and inorganic electroluminescence (EL) microparticles for direct visualization of input sound signals. Field-induced EL of the microparticles in the device depends upon the source sound wave, making their EL synchronized with sound arising from the piezoelectric actuation. The flexible artificial synesthesia devices with sound-synchronized EL (FASSEL) showed extreme mechanical tolerance that can be repeatedly folded and crumpled with visible sound, allowing a variety of unexplored applications including synchronous sound-lightings and wearable, on-body sound-vision systems to facilitate emotional interaction of human being with sound in a human-friendly form.

1. Introduction

Development of stimuli-interactive display capable of spontaneously visualizing various external human sensible inputs has been of great interest and tremendous efforts are devoted to the visualization of nonvisible human senses such as touch, smell, taste, and sound with potentials in numerous Internet of Things applications [1–6]. Most of the studies focus on visualization of the stimuli related to touch, which human skin is responsible for, including pressure [7–10], temperature [11], and conductance [12]. These interactive displays generally incorporate active sensor arrays to achieve efficient stimuli-interfacing, as well as optical elements for visualizing the stimuli based on a variety of smart materials of pneumatic microfluidic networks [13,14], organic electrochromics [15], electroluminescence (EL) [16], and thermochromics [17,18]. In particular, EL of organic and/or inorganic phosphors is frequently employed due to their self-emitting characteristics as well as high brightness and efficiency [19–21].

In spite of extensive studies conducted on visualization of touch owing to the great interest in realizing flexible electronic skin, no attention in this flexible thin film device field was paid to visualization of continuous sound waves that are much more complicated than human touch. The visualization of sound in a flexible form of devices is technologically useful with numerous potential applications including the visible assistance for people with hearing problems, the efficient sound recognition in noisy environment for safety purposes and medical applications utilizing sound-to-vision conversion in addition to esthetic entertainment purposes. The sound visualization is accomplished in which electrical sound signals of alternating current (AC) fields with different frequencies [22–25] can be responded with an optical element, giving rise to light emission with brightness levels and colors corresponding to different sound octaves and volumes.

One would imagine that it can be realized by connecting two independent display and loudspeaker elements in parallel and to make the display element responsive to sound signals from the loudspeaker.

* Corresponding author.
E-mail address: cmpark@yonsei.ac.kr (C. Park).
[1] These authors contributed equally to this work.

https://doi.org/10.1016/j.nanoen.2019.03.006
Received 23 October 2018; Received in revised form 19 February 2019; Accepted 2 March 2019
Available online 07 March 2019

The approach can, however, apparently require additional accessories and/or complicated circuit design to convert the sound signals to electrical ones to which the display can respond. It would be, therefore, desirable if sound generation and visualization occur in a single, flexible thin film device that can offer an artificially stimulated sound-vision synesthesia; in other words, the development of a flexible electronic device via visualization of sound, so called "visible sound" as an example of artificial synesthesia systems can be a new type of electronics which people can easily carry for safety, health-care, and entertainment purposes. We envision that this issue can be addressed by an elaborate design of composite materials where inorganic phosphors embedded in an electrically insulating and piezoelectric polymer can give rise to field-induced EL responsive to AC based sound signals, allowing for a flexible artificial synesthesia devices with sound-synchronized EL (FASSEL) which also takes an advantage of its mechanical flexibility.

Herein, we demonstrate a thin-film-based FASSEL that enables sound visualization. The FASSEL is made of a thin polymer composite of a piezoelectric poly(vinylidene fluoride-co-trifluoroethylene) (PVDF-TrFE) and field-induced light-emitting ZnS microparticles and responsive to continuous AC sound input signals. During signal-dependent sound generation in the composite film due to the piezoelectric actuation of the PVDF-TrFE [26], EL also occur simultaneously due to the solid-state cathode luminescence of ZnS depending upon the AC fields [27,28], giving rise to a high-performance sound-synchronized EL in a single device. Both field-induced EL intensity and the color of the light emitted by the FASSEL are closely correlated with sound amplitude and frequency. The effective piezoelectric sound generation synchronized with EL emission was achieved by carefully adjusting the poling field, annealing temperature, and amount of ZnS microparticles encapsulated with the controlled silica shells. By employing transparent polymer electrodes, we developed a mechanically flexible, foldable, and even crumpled FASSEL whose shape can be readily altered without significant performance degradation, enabling various unconventional applications of stand-alone lighting speakers, origami-foldable ones and skin-mountable EL ones.

2. Experimental section

2.1. Materials

Green ZnS (D512S, ZnS:Cu), orange (D611S, ZnS:Cu, Mn), blue (D417S, ZnS:Cu, Al) microparticles were purchased from Shanghai KPT Co. Poly(vinylidene fluoride-co-trifluoroethylene) (PVDF-TrFE) was purchased from SOLVAY (250/P400). The modified PEDOT:PSS (Clevios PH 1000) by mixing with Zonyl surfactant (FS-300 fluorosurfactant) and dimethyl sulfoxide (DMSO) was purchased from Sigma-Aldrich. Poly(dimethylsiloxane) (PDMS) and cross-linker were purchased from Dow Corning. All other materials were purchased from Sigma-Aldrich and used as received.

2.2. Silica encapsulation on ZnS microparticle

For improving both EL and sound generation properties, a thin silica layer was coated on a ZnS microparticle based on the Stober method. First, 2.0 ml of TEOS, 5.0 ml of ethanol and 10.0 ml of distilled water was mixed together at room temperature. The mixture was carefully adjusted to 8.0 in pH by adding NH_3 solution for 10 min at 70 °C. Then silicic acid solution was slowly injected into the suspension of 5.0 g of ZnS microparticles in 50 ml of distilled water mixed with 60 µl of 3-aminopropyltrimethoxysilane (APTMS). The mixture was stirred for 3 h at 50 °C. After washed 5 times, followed by being baked for 1 h at 150 °C, silica encapsulated ZnS microparticles were developed with different silica thickness dependent upon the initial concentration of TEOS.

2.3. Fabrication of a FASSEL

Our FASSEL was fabricated by all solution-based processes as shown in Fig. 1a (Table S1 and Fig. S1a). First, a Si wafer substrate was sequentially cleaned twice, with acetone and 2-propanol in an ultrasonic bath for 10 min each, followed by UV treatment for 15 min. PVDF-TrFE powders and silica-encapsulated (SE)-ZnS microparticles were dissolved in MEK solvent and stirred at 75 °C and with 450 rpm for 2 h. A solution of PVDF-TrFE with various concentrations of SE-ZnS microparticles with an average diameter of 8 µm was spin-coated onto the Si wafer substrate, followed by thermal annealing at 140 °C for 2 h in glove box, leading to an approximately 20 µm-thick composite film. To ensure the efficient EL performances of ZnS particles in piezoelectric polymer medium, the ZnS microparticles were encapsulated with thickness-controlled silica based on sol-gel method [29–31]. The composite of approximately 20 µm thickness is mechanically flexible and optically translucent as shown in Fig. 1a. High-conductivity PEDOT:PSS was modified by mixing it with 5 wt% DMSO and 0.5 wt% Zonyl surfactant with respect to PEDOT:PSS. A PEDOT:PSS layer was then spin-coated from the modified solution on the composite film. An approximately 400-nm-thick PEDOT:PSS film was subsequently annealed at 110 °C for 1 h in ambient atmosphere. Both composite and PEDOT:PSS layers were mechanically transferred on a PDMS film coated on a Si wafer to ensure the flatness of the composite/PEDOT:PSS films. Another PEDOT:PSS film was spin-coated on the transferred composite/PEDOT:PSS film, followed by thermal treatment at 110 °C for 1 h, giving rise to a PEDOT:PSS/PVDF-TrFE with SE-ZnS composite/PEDOT:PSS capacitive-type film speaker with firm interfaces between electrode and composite as shown in Fig. 1c. Device fabrication was completed when the two PEDOT:PSS electrodes were electrically connected as shown in a Fig. S1a.

2.4. Cross-sectional morphology and crystalline characterization

The cross-sectional morphology and thickness of PVDF-TrFE with SE-ZnS composites were characterized by using a field-emission scanning electron microscope (FESEM) (JEOL-7800F) as shown in Fig. 1c. The morphologies of SE-ZnS particles were obtained using focused-ion-beam transmission electron microscopy (FIBTEM) (JIB-4601F, JEOL). FT-IR (VERTEX 70) and X-ray photoelectron spectroscopy (XPS) (K-alpha) were used to characterize the silica layers on ZnS microparticles. In addition, the information related to crystal of PVDF-TrFE and composite films was obtained using high resolution X-ray diffractometer (HR-XRD) (Smart lab) and grazing incidence wide angle X-ray scattering (GISAXS) (Pohang Accelerator Laboratory). SE-ZnS microparticles with the size distribution resulted in composite films with large surface roughness (Fig. S3b).

2.5. Electrostatic simulation

Electrostatic field simulation was performed using finite element analysis software, Elmer (CSC – IT Center for Science). To simplify the simulation, ZnS:Cu particle was depicted as circular shape. Interface between electrode (PEDOT:PSS) and PVDF:TrFE was set to constant potential boundary and the rest of electrode was not considered in the simulation. Potential difference between two electrode was 100 V. Dielectric constants of ZnS:Cu, PVDF:TrFE and SiO_2 were set to 500, 11 and 3.9, respectively.

2.6. A thin piezoelectric FASSEL characterization

The sound characterization of a FASSEL is illustrated in a Fig. S2a. The white noise signal of full frequency range from a commercial smartphone was amplified by an amplifier (GNS MA-220) and entered into the FASSEL in the form of AC field signals as shown in Fig. 1d. To measure the sound pressure arising from piezoelectric actuation of the

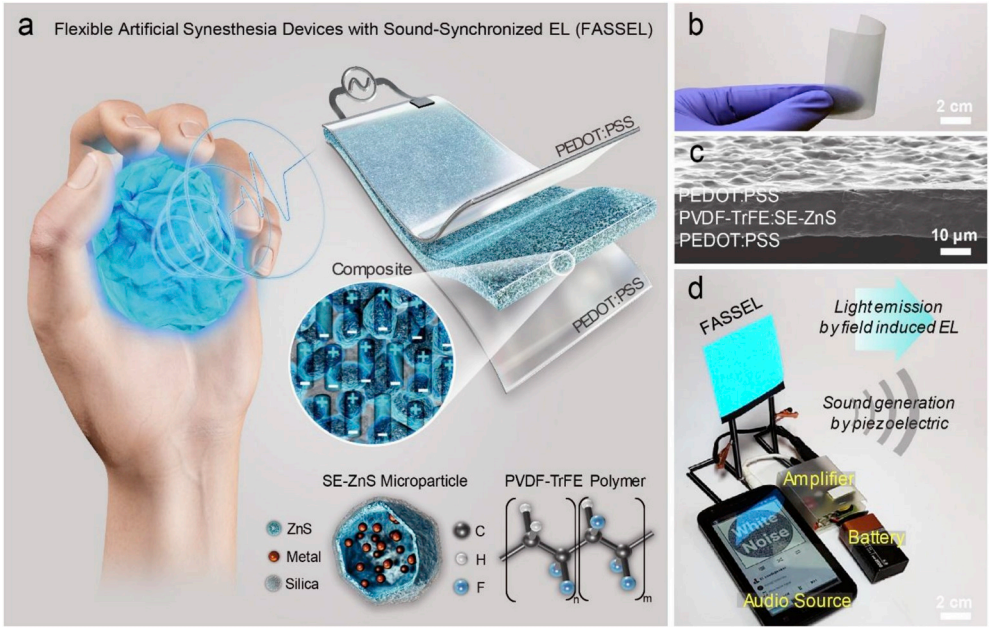

Fig. 1. Thin piezoelectric film-based flexible artificial synesthesia device with sound-synchronized electroluminescence (FASSEL). (a) Conceptual illustration and schematic of a thin, FASSEL consisting of three layers of PEDOT:PSS, PVDF-TrFE with SE-ZnS microparticles, and PEDOT:PSS. (b) A photograph of the FASSEL over a large area (7 × 7 cm^2). (c) A cross-sectional SEM image of the device. (d) A photograph of a FASSEL developed with the operation system. The AC field amplified from an audio source and applied to the FASSEL gives rise to simultaneous field-dependent light-emission and sound generation arising from solid-state cathode luminescence of SE-ZnS microparticles and piezoelectric actuation of PVDF-TrFE, respectively.

FASSEL in response to the AC field signals, an omnidirectional microphone (Earthwork M23) was used and positioned at 100-mm distance from the device (Fig. S2b). The output sound signals produced from the FASSEL were converted to digital sound signals, and amplified by an audio interface (TASCAM US 2X2). The digital sound signals with waveforms in the time domain were converted to those in the frequency domain by fast Fourier transform (FFT) of a spectrum analyser (SIA Smart live) of a desktop computer. Both the sound detection angle and the frequency-dependent SPL were measured in the frequency range from 20 Hz to 20 kHz that covers the range that the human ear can recognize. All SPL data were acquired by averaging the output signals for 10 s, discluding the environment noise data to minimize an external noise effect as shown in a Figs. S7a and S7b. In an angle-dependent SPL measurement of the FASSEL, The device was fixed, while the microphone was rotated. The size of the active area of the FASSEL for sound measurement was 6.25 cm^2 (25 mm × 25 mm).

2.7. Characterization of EL performance and piezoelectric polarization

Field-induced EL results from the solid-state cathode luminescence of SE-ZnS microparticles in the composite film due to the AC source signals, and the brightness and color of the sound-synchronized EL are characterized by a spectroradiometer (Konica CS 2000). A function generator (Agilent 33220A) connected with a high-voltage amplifier (TREK 623B) was used for high-voltage poling and EL driving of the FASSEL. The piezoelectric polarization of the composite film was characterized with RT66. All measurements were performed in a dark box under ambient conditions in air. The size of the active area for EL measurement was 6.25 cm^2 (25 mm × 25 mm).

3. Results and discussion

Since it was critical to avoid possible electrical leakage arising from the semiconducting ZnS microparticles distributed in a composite film which could lead to significantly deteriorated polarization of the piezoelectric film, the surface of the microparticles were encapsulated with thickness-controlled silica layers by varying the amount of tetraethyl orthosilicate (TEOS) precursor from 1 to 10 wt% (Fig. S3). The transmission electron microscopy (TEM) images in Fig. 2a shows that 20 nm thick silica is uniformly coated on ZnS microparticles (Fig. S3b). The X-ray photoelectron spectroscopy (XPS) of SE-ZnS microparticles also shows that silica is well formed on surface of ZnS microparticles as shown in Fig. 2B. The Zn 3p and S 2p peaks at 89 and 162 eV of SE-ZnS microparticles were substantially reduced while the Si 2s and Si 2p at 154 and 103 eV peaks were increased [32]. The encapsulation of ZnS particles with silica layer was critical for ensuring the high performance of both sound and EL.

The current density–voltage characteristics were examined of metal/composite film with SE-ZnS microparticles/metal capacitors as a function of silica thickness as shown in Fig. 2c. The current density was drastically decreased with the silica layer, but rarely altered when SE-ZnS microparticles were employed with their thickness greater than 20 nm (3 wt% sample). Consistent with the current density results, the sound pressure level (SPL) of the devices was poor with the silica layers less than 20 nm, compared with that of a device containing a pristine PVDF-TrFE film due to possible electric leakage. SPL was comparable with that of a PVDF-TrFE film when SE-ZnS microparticles were employed with their thickness greater than 20 nm (3 wt%) as shown in Fig. 2d. It is noted that the PVDF-TrFE crystal orientation is rarely affected by the presence of the SE-ZnS microparticles (Fig. S4c). The light emission performance of our composites as function of silica thickness is also consistent with the results of both current density and SPL, as shown in Fig. 2e. The luminance of a device was significantly increased with the silica layer up to 20 nm in thickness due to the effective suppression of leakage current. The EL intensities of devices were decreased with the silica layer thicker than 20 nm due to the lowered electric field arising from the thick insulating silica layer at the same operation voltage. The devices with the silica layers thinner than 20 nm were often broken down at the 2 kV while ones with SE-ZnS microparticles greater than 20 nm in thickness were rarely broken down, as shown in Fig. 2f.

In order to confirm the effect of silica encapsulation on the reduction of leakage current, we performed electrostatic field calculation and the results are shown in Fig. 2g, h and i. A structural model composite was built to simulate the composites examined experimentally in terms of morphology, film thickness and operation voltage. Two model composites were made containing neat ZnS and SE-ZnS particles, respectively. In both composites, the particles were randomly dispersed and some particles were in contact with each other as representatively shown in the composite containing SE-ZnS particles in Fig. 2g. When voltage was applied of 100 V across the two electrodes, both composites showed electric field concentrated at the edges of ZnS particles as

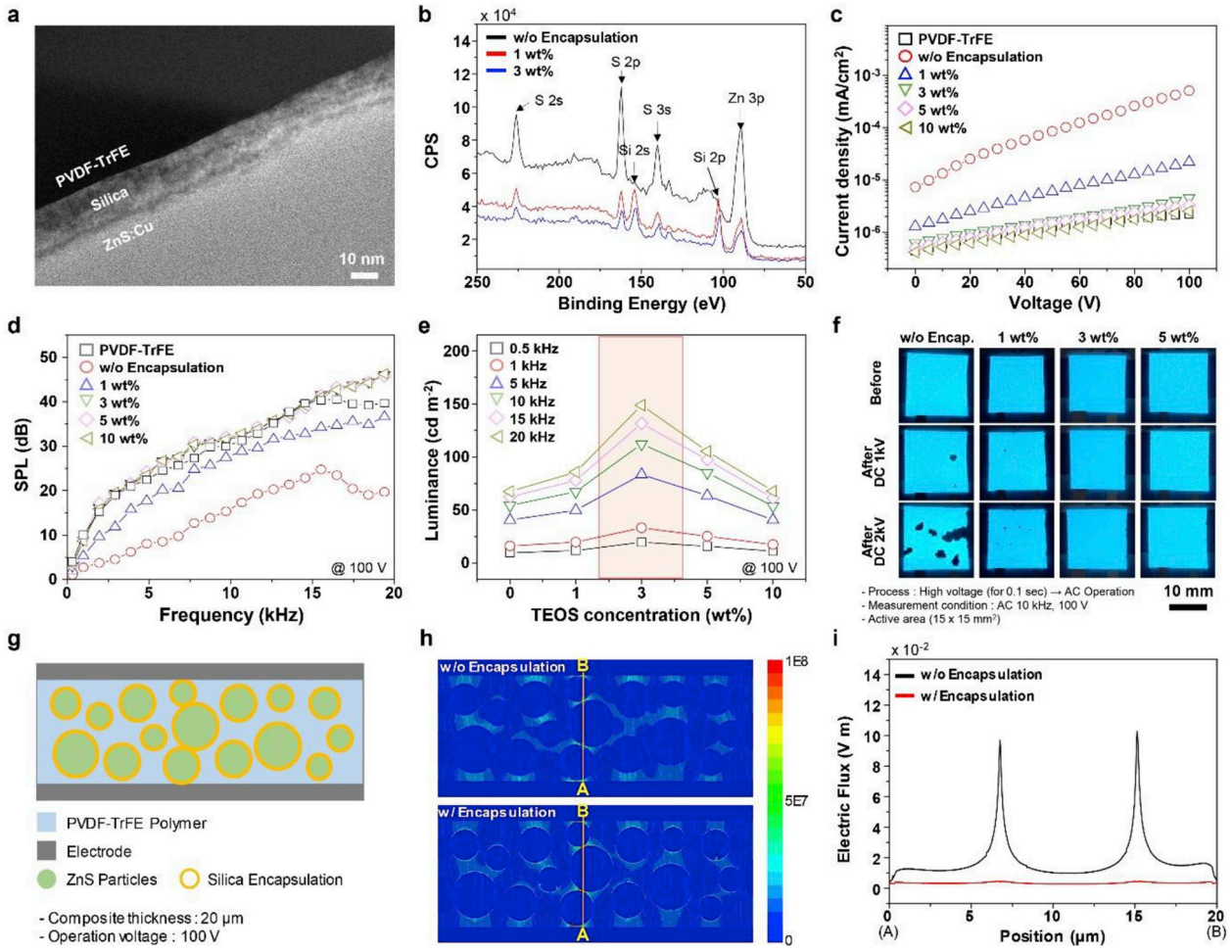

Fig. 2. Optimization of silica encapsulation on ZnS microparticles. (a) A bright field TEM image of SE-ZnS particle prepared with 3 wt% TEOS with respect to ZnS particles. The silica layer is approximately 20 nm in thickness. (b) XPS spectra of SE-ZnS particles prepared with different TEOS concentrations. (c) Current density versus voltage (J–V), (d) SPL versus AC frequency of FASSELs with SE-ZnS particles prepared with different concentrations of TEOS with respect to ZnS particles. (e) Luminance characteristics as a function of the contents of TEOS with respect to ZnS particles. (f) Photographs of EL images of the FASSELs with SE-ZnS particles prepared at different TEOS concentrations before and after high voltage pulses for 0.1 s. The EL images were obtained at the AC frequency of 10 kHz and the voltage of 100 V. (g) Schematic of composite model of SE-ZnS particles in PVDF-TrFE for electrostatic simulation. 2D electric field distribution maps (h) and electric flux plots across A and B position (i) of two model composite films containing uncoated-ZnS and SE-ZnS particles. All the samples contain the 20 μm thick composite films with 60 wt% ZnS particles with respect to PVDF-TrFE.

shown in Fig. 2h. More severe field concentration was observed in the composite containing neat ZnS particles. The electric flux results across a and b position of the two composite films in Fig. 2i show that significant field concentration occurred at the two contact points of the neat ZnS particles while electric field was not much developed with the SE-ZnS particles. The simulation results also support our argument that silica encapsulation reduces leakage current between ZnS particles, giving rise to high performance FASSEL.

To further enhance the SPL of our FASSEL which strongly depends upon the piezoelectric polarization of PVDF-TrFE, the electric poling process was employed, as shown in Fig. 3a (Figs. S5 and S6) [33]. The SPL of approximately 30 dB of an un-poled PVDF-TrFE (point 1 of Fig. 3a and b) was rapidly increased when a positive voltage was applied in the device over approximately 900 V, which corresponded to approximately 60 MV/m (point 2 of Fig. 3a and b). The enhancement of the SPL arises from preferred polarization built in the composite as evidenced in the polarization–voltage results of the capacitor in Fig. 3b. The SPL was saturated to approximately 56 dB at the applied voltage of 1600 V (point 3 of Fig. 3a and b). The SPL was preserved even after the removal of the applied voltage owing to the remnant polarization of PVDF-TrFE (point 4 of Fig. 3a and b). The SPL rapidly decreased and minimized with the voltage of −900 V because of the neutralized polarization (point 5 of Fig. 3a and b). The large SPL observed with the applied voltage of 1600 V was fully recovered with the voltage of −1600 V, which implies that the SPL does not depend upon the direction but the amount of polarization of PVDF-TrFE (point 6 of Fig. 3a and b). Again, when the voltage was removed, the large SPL still remained (point 7 of Fig. 3a and b). Another SPL minimum was observed when the polarization direction was switched at the coercive voltage of approximately 900 V (point 8 of Fig. 3a and b). Again, the saturated SPL was obtained with the 1600 V poling (point 9 of Fig. 3a and b). Since the piezoelectric polarization is proportional to the degree of crystallization of PVDF-TrFE, the SPL was further enhanced with thermal annealing that allowed additional crystal growth in PVDF-TrFE at temperatures below the melting point of PVDF-TrFE (~146 °C) (Figs. S6a and S6b). It should be noted that the voltage imposed to a device up to ± 1600 V was used for electrical poling of a PVDF-TrFE film while the operation of a device was made at the voltage lower than 150 V.

The resulting FASSEL with electrically poled and thermally annealed PVDF-TrFE exhibits excellent SPL that is better than that with an un-poled PVDF-TrFE film over a broad range of sound frequencies, including the range that the human ear can hear, when white noise input signal was applied at 100 V as shown in Fig. 3c (Fig. S7a). One of the advantages of a thin piezoelectric FASSEL is that sound is uniformly

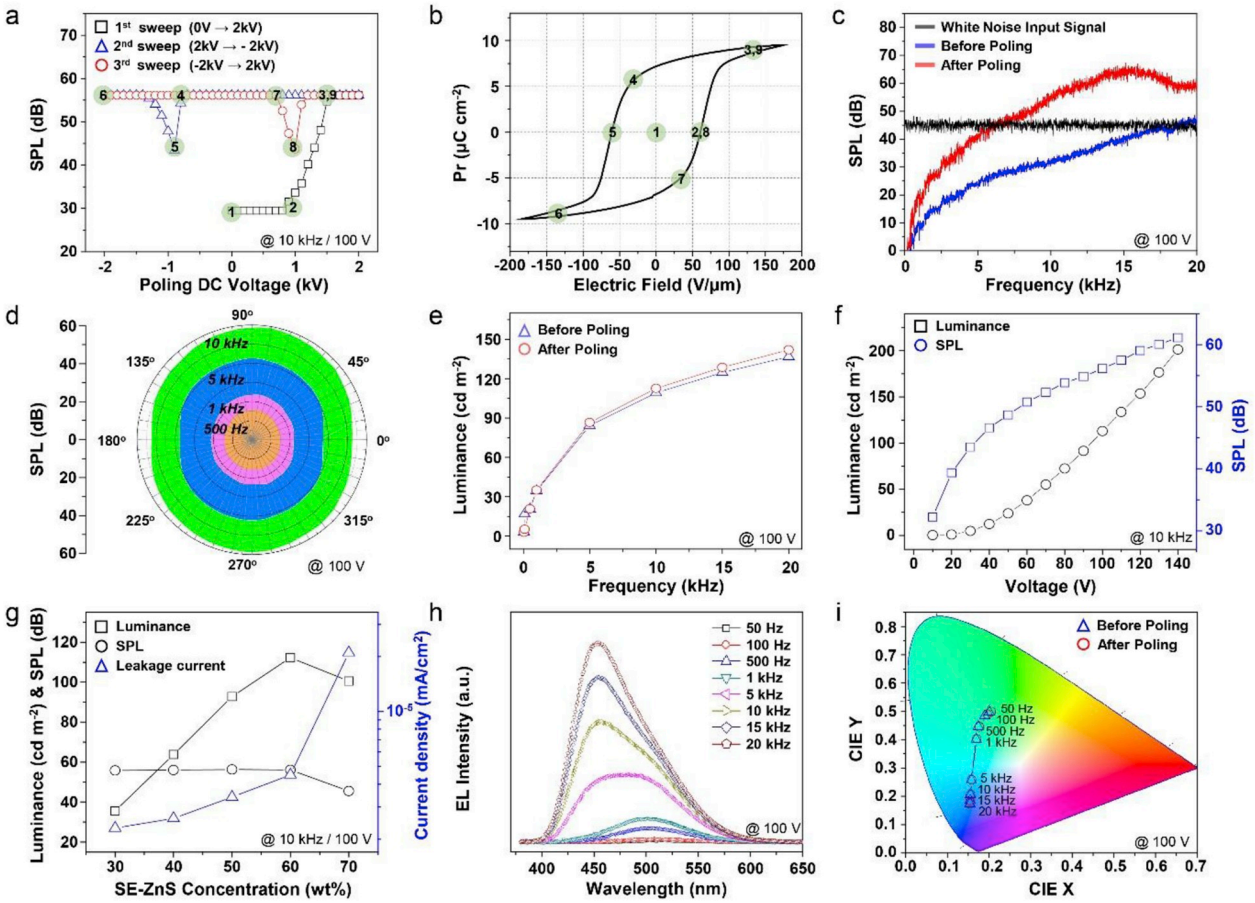

Fig. 3. Sound and EL characterization of the FASSEL. (a) A plot of SPL as a function of the DC poling voltage of the FASSEL. SPL was measured at the AC frequency of 10 kHz and the voltage of 100 V. (b) The polarization versus electric field of the FASSEL. Each number (1–9) of Fig a and Fig b represents SPL and polarization in same electric field. (c) SPL frequency spectrum measurements of poled and un-poled PVDF-TrFE films over the range of sound frequency from 10 Hz to 20 kHz using white noise signal source. (d) Angle-dependent SPL of the FASSEL as a function of frequency at the operating voltage of 100 V. (e) Luminance versus frequency (L–F) characteristics of poled and un-poled FASSELs at the AC voltage of 100 V. (f) Luminance and SPL of the device as a function of AC voltage at the AC frequency of 10 kHz. (g) Variation of luminance, SPL at the AC frequency of 10 kHz, voltage of 100 V and leakage current at DC voltage of 100 V of FASSELs as a function of contents of SE-ZnS microparticles with respect to PVDF-TrFE. EL spectra (h) and CIE coordinates (i) of the FASSEL as a function of AC frequency at the AC voltage of 100 V. The samples are 20 μm in thickness and contain 60 wt% SE-ZnS particles with respect to PVDF-TrFE.

generated regardless of the detection angle. This detection angle-independent sound generation was confirmed with our FASSEL on a rotating stage and the results in Fig. 3d show that the SPL at each representative frequency is similar irrespective of the detection angle (Fig. S7c).

The field-induced EL from SE-ZnS microparticles was independently examined as a function of frequency at 100 V as shown in Fig. 3e. Consistent with the previous results of AC EL devices with ZnS microparticles [34–39], our composite also shows that the luminance increases in the frequency range corresponding to that of sound input signals. While poling of a composite significantly improved SPL with the sound input signals, no significant difference was observed in the behavior of frequency-dependent luminance, which clearly implies that SE-ZnS particles are solely responsible for EL. Both luminance and SPL increase with applied voltage at a fixed frequency as shown in Fig. 3f. The results suggest that the volume of sound from the FASSEL is, in principle, directly recognized with the brightness of EL. The EL of our FASSEL depends upon the amount of SE-ZnS particles as shown in Fig. 3g (Fig. S8). EL performance was enhanced with SE-ZnS particles up to 60 wt% with respect to PVDF-TrFE, above which the performance was adversely affected. The thickness of the composite film was also optimized to approximately 20 μm and the film showed the best EL performance without adversely affecting the sound generation performance (Fig. S9). EL performance of a capacitive type, field induced EL device based on AC operation is significantly degraded with the leakage current. In our system, the EL performance was improved with the amount of SE-ZnS due to the increased carriers in a unit volume of the composite. The higher EL was achieved, the thinner composite film with a given SE-ZnS content. In addition, the higher EL, the greater content of SE-ZnS in a composite with a given thickness. The leakage current, at the same time, increases when a film becomes thinner with a given SE-ZnS content as well as when SE-ZnS content increases in a given film thickness due to insufficient encapsulation of SE-ZnS particles with PVDF-TrFE (Figs. S8 and S9). The detailed sound and EL performance of our FASSELs are summarized in Table 1.

In addition to luminance change as a function of sound frequency, our FASSEL allows for frequency-dependent color alteration as shown in Fig. 3h [40,41]. The frequency dependent color changes observed with the various ZnS particles is mainly ascribed to the various trap energy levels developed during doping process. Carriers from the ground state are first excited to the conduction band of ZnS, and subsequently move to the lower trap energy levels, followed by the light emission corresponding to the gap between ground and trap level state. The movement of the carriers from the conduction band of ZnS and the trap level is frequency-dependent, resulting in color variation as a function of applied frequency. The theoretical background of the frequency-dependent emission is well developed [42,43]. The wavelength at the maximum brightness of an EL spectrum is clearly blue-shifted

Table 1
Sound and EL characteristics of PVDF-TrFE composites with SE-ZnS microparticles.

Classification	Condition		Luminance	SPL	Current density	Dielectric constant
			(cd/m^{-2})	(dB)	(mA/cm^2)	ε_r
	Value	Poling	@ 10 kHz/100 V	@ 10 kHz/100 V	@ 100 V	@ 10 kHz
Surface coating (wt %)	0	X	54.3	16.3	5.1E-04	14.2
	1		67.4	28.2	2.0E-05	13.2
	3		109.1	31.9	4.6E-06	12.7
	5		85.1	32.5	3.3E-06	12.7
	10		53.8	32.2	2.5E-06	12.7
Contents of SE-ZnS (wt %)[a]	0	O	–	55.4	2.2E-06	10.9
	30		35.6	55.8	2.3E-06	11.2
	40		63.8	56.0	2.6E-06	12.0
	50		92.8	56.3	3.4E-06	12.3
	60		112.3	56.1	4.5E-06	12.7
	70		100.5	45.5	2.0E-05	13.9
Film Thickness (μm)	12	O	89.2	34.7	3.0E-05	13.6
	16		104.6	52.9	8.3E-06	12.9
	20		112.3	56.1	4.5E-06	12.7
	24		74.0	54.5	2.8E-06	12.6
	28		37.4	42.2	2.2E-06	12.5

[a] SE-ZnS particles have the silica layers of approximately 20 nm in thickness.

with the frequency at 100 V. The maximum wavelength of approximately 520 nm at 50 Hz became 450 nm at 20 kHz, making our FASSEL color-tunable from green to blue depending on the sound frequency as shown in the CIE plot of Fig. 3i. The detailed EL and sound output performance of a FASSEL with the input AC sound signals were summarized in Table 2.

The metal-doped ZnS particles can be considered as a p-type semiconductor. The color of metal-doped ZnS particles is determined by the characteristic energy levels controlled by dopants. For instance, Mg, Cu and Al energy state related emission is expected at a lower energy position as compared to the band energy absorption of ZnS. Mg, Cu and Al substitute Zn ions in ZnS crystals introducing a trap energy level, where electron and hole can be trapped. The EL emission could be attributed to the radiative decay between those localized states of Mn, Cu and Al inside the ZnS band-gap. The metal-doped ZnS particles emitting blue, green and orange under AC field [44,45]. The FASSEL with blue and orange SE-ZnS particles in PVDF-TrFE were also fabricated (Fig. S10). The device containing either blue or orange SE-ZnS particles exhibits frequency-dependent color-tunable light emission, similar to that observed with the green particles, allowing for a broad full visible range color control with sound. To rule out the possible thermoacoustic sound generation arising from PEDOT:PSS electrodes [46], we fabricated the FASSEL with aluminum electrode (Fig. S11a). We observed the SPL performance similar to that with PEDOT:PSS, which indicates that SPL of our device mainly arises from the piezoelectricity of PVDF-TrFE. The surface temperature of the two devices with Al and PEODT:PSS electrodes was rarely varied with the frequency, which supports our argument of the piezoelectric sound generation (Fig. S11b).

It is important to examine how directly the EL of our FASSEL is correlated with sound for further utilization of our FASSEL as a synchronous sound-EL display. For the purpose, we chose six different octave piano sounds with their major sound frequencies ranging from low to high as shown in Fig. 4a and converted them into AC input sound signals (Fig. S12a). The input signals applied to our FASSEL produced six distinguishable SPL versus frequency sound spectra as shown in

Table 2
EL and piezoelectric sound characteristics of a FASSEL with the input AC signals.

Control Factor	Input		Output			
	Electric source (AC)		Electro-luminescence		Piezoelectric sound	
	Voltage (V)	Frequency (Hz)	Luminance (cd/m^{-2})	Wavelength (nm)	SPL (dB)	Octave/Note
Voltage	20	10000	1.1	505	39.4	9/D#
	40		12.5		46.6	
	60		38.0		50.7	
	80		72.5		52.2	
	100		112.3		56.1	
	120		153.5		59.0	
	140		201.2		61.1	
Frequency	100	50	2.8	448	2.7	1/G#
		100	5.1	450	5.6	2/G#
		500	20.7	456	15.0	4/B
		1000	35.0	471	20.3	5/B
		5000	86.6	481	41.3	8/D#
		10000	112.3	502	56.1	9/D#
		15000	128.6	509	64.7	9/A#
		20000	142.0	520	57.9	10/D#

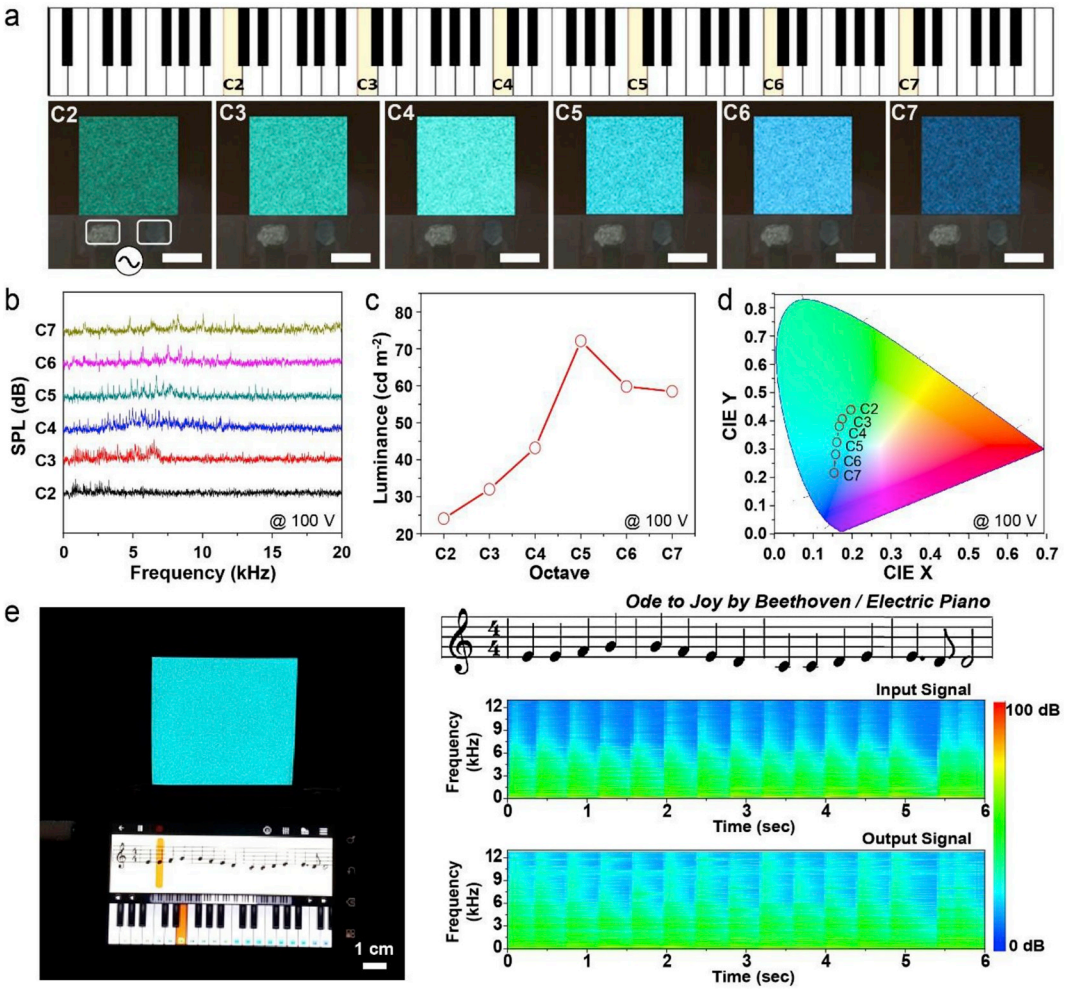

Fig. 4. Loudspeaker performance of the FASSEL. (a) Photographs of EL images of the FASSEL containing 60 wt% SE-ZnS particles with respect to PVDF-TrFE with different colors arising from six-scale "do" octave input sources of an electric piano as shown in the scheme of a piano keyboard. (b) SPL versus frequency sound spectra as a function of octave at the electric piano input signal of each octave and the voltage of 100 V. (c) Luminance characteristic and (d) CIE coordinates of the FASSEL under six different octave input sources of the electric piano and the voltage of 100 V. (e) Demonstration of music 'Ode to Joy' by the FASSEL. A photograph of the FASSEL with electric piano score and keyboard (left). The input and output sound signals with different SPLs in frequency versus time domains are shown (right). All scale bars are 1 cm. (For interpretation of the references to color in this figure legend, the reader is referred to the Web version of this article.)

Fig. 4b. At the same time, our FASSEL exhibited EL with different colors that depended upon the octaves as representatively shown in the photographs of Fig. 4a. The CIE plot in Fig. 4d clearly shows that the individual octave piano sounds correspond to different colors. The luminance of EL at each octave was also varied, depending upon the octave. Luminance increases with octave and slightly decreases at high octaves of C6 and C7 mainly due to their vibration periods shorter than those for the others when we chose a voltage of 100 V, respectively, as shown in Fig. 4c. Music recorded as AC sound input signals was successfully reproduced with EL variation, depending upon sound notes as shown in Fig. 4e. The song, "Ode to Joy" recorded by an electric piano, was first converted into AC input sound signals with different SPLs in frequency versus time domain. The input signals were almost identically reproduced through our FASSEL, giving rise to the output sound signals as shown in the right bottom of Fig. 4e. As expected, while playing the music, the FASSEL exhibited various colors with different brightness (Video S1).

Supplementary data related to this article can be found at https://doi.org/10.1016/j.nanoen.2019.03.006.

Our FASSEL consisting of a polymer composite with top and bottom PEDOT:PSS electrode with fluoro-surfactant [47,48] is additionally beneficial because of its mechanical flexibility, making it suitable for applications requiring various types of mechanical deformation such as bending, folding, and crumpling as shown in Fig. 5. To ensure further mechanical reliability, both sides of our FASSEL were coated with thin PDMS layers (Fig. S13a). We confirmed that piezoelectric actuation of PVDF-TrFE as well as EL of SE-ZnS microparticles in our FASSEL were hardly affected by the elastomeric and transparent PDMS layers (Figs. S13a and S13b). Delamination of the constituent layers hardly occurred by the encapsulation of a device with elastomeric PDMS. Not to mention that our FASSEL with synchronous sound and EL was successfully operated upon severe bending with both luminance and SPL rarely altered as a function of bending radius (Fig. S14a). Even after our device was folded 20 times, no significant degradation in performance was observed, as shown in Fig. 5a (Fig. S14b). Piezoelectric potential should be stress-dependent and thus different piezoelectric polarization states would be developed, depending upon localized stress during the mechanical deformation of bending, folding and crumpling [49,50]. It is, however, unfortunate that we were not able to examine the SPL at the localized area due to the limitation of our experimental facility. SPL values we obtained after mechanical deformation were ones averaged out with whole film area of approximately 25 cm^2. All SPL values were obtained in the re-flattened state after mechanical deformation.

More interestingly, our mechanically robust FASSEL worked reliably under repetitive crumpling by hand as shown in Fig. 5b. After 10 crumpling events, the device performance was similar to that before

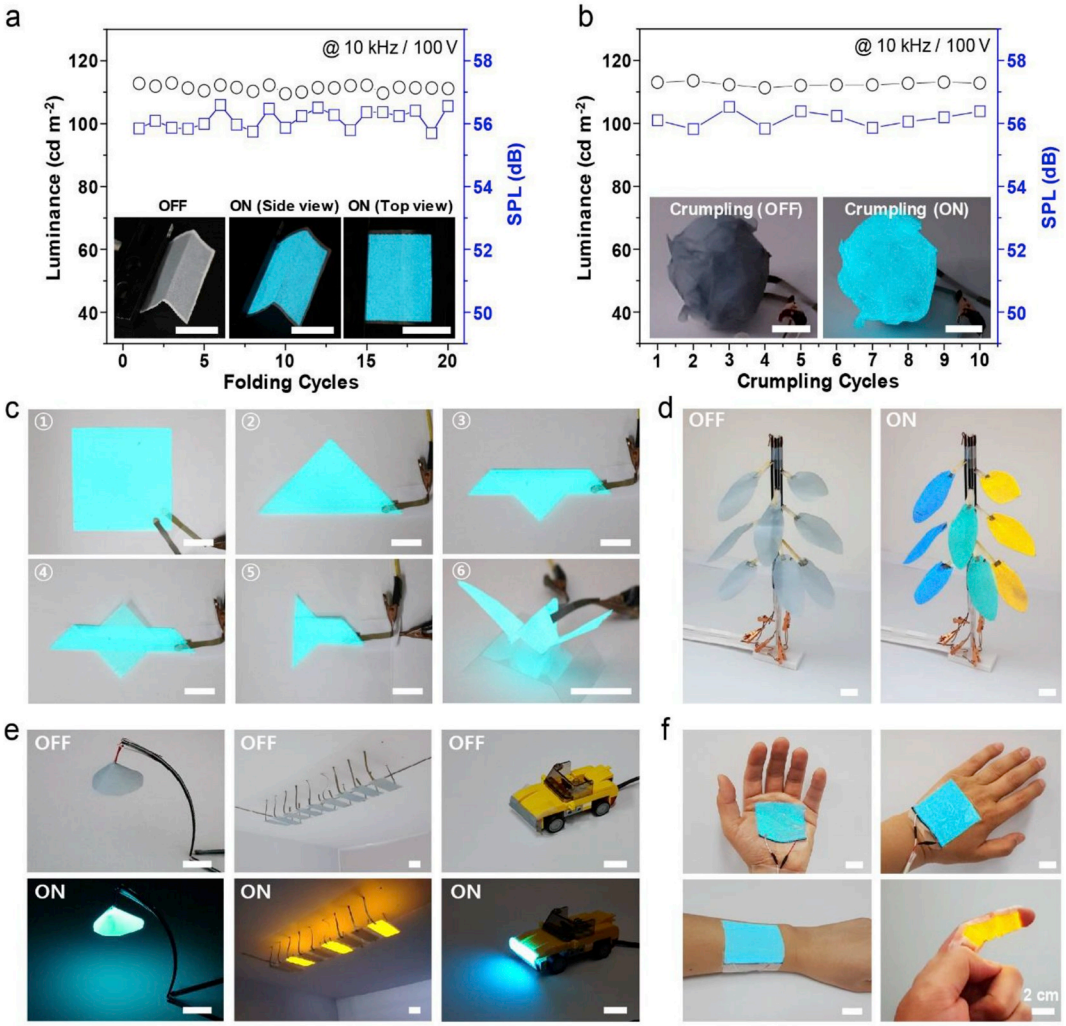

Fig. 5. Mechanically robust FASSEL with various applications. (a) Luminance and SPL characteristics of the FASSEL as a function of the number of folding cycles. Photographs of the folded device are shown in the inset. (b) Luminance and SPL characteristics of the FASSEL as a function of the crumpling cycles. All tests were performed at the AC frequency of 10 kHz and the voltage of 100 V. Photographs of a crumpled device in OFF- and ON-state are shown in the inset. (c) Photographs showing the fabrication steps of an origami bird FASSEL which was successfully developed in 6th step. (d) Photographs of a full color EL decoration of a tree FASSEL. (e) Photographs of various unconventional usages of the FASSEL including a stand-alone desk lamp speaker, a miniaturized room lighting speaker and a toy car head lamp one with horn function. (f) Photographs of skin-mountable FASSEL worn on various parts of body. All scale bars are 2 cm. (For interpretation of the references to color in this figure legend, the reader is referred to the Web version of this article.)

crumpling. The sample was subsequently re-crumpled and re-flattened, followed by the SPL measurement. Since the folded or crumpled areas are relatively small, compared with undeformed area of a FASSEL, the SPL from the device was rarely changed even after multiple folding and crumpling events. The ZnS particle density (or the distance between the particles) may be lowered in the upper part while the density is increased in the lower part. Considering that AC field is exerted between top and bottom electrode, the average particle density may, however, remain same at the bent location, resulting in the light emission similar to that observed in undeformed areas. In fact, the light intensity was rarely varied, in particular, at the deformed areas in our experimental conditions. The coated elstomeric layer firmly adhering to a fragile polymeric layer rendered the fragile film micro-fractured [51,52]. When the elastomic layer was recovered after mechanical deformation, the micro-fractures in the fragile film were also partially recovered, giving rise to the electrical performance quite similar to that before the deformation (Figs. S15a and S15b). In our FASSEL, we have observed that the device performance was significantly degraded upon mechanical deformation mainly due to the fractures in PEDOT electrodes without PDMS layers (Figs. S16a and S16b). The operation reliability of the FASSEL with time is an important aspect. While no significant deterioration in SPL was observed when the operation lasted longer than 100 h, the luminance decreased with time. The device showed a half-life time in luminance of approximately 50 h (Fig. S17a). The lifetime can be further improved by incorporating suitable passivation technologies into the top and bottom substrates.

The excellent reliability of our FASSEL under various mechanical deformations allowed us to fabricate unconventional film FASSEL s with a variety of three-dimensional geometries and shapes. Representatively, we successfully demonstrated a bird origami of our FASSEL as shown in Fig. 5c. Besides every folding step, the origami bird FASSEL performed well with excellent simultaneous sound generation and EL, as shown in the photographs of Fig. 5c (Video S2, Supporting Information). The mechanical robustness of our FASSEL also allowed us to demonstrate its various unconventional usages including a full color EL decoration tree speaker (Fig. 5d), a stand-alone desk lamp speaker (the left of Fig. 5e), a miniature room lighting speaker (the middle of Fig. 5e) and a toy car's head lamp speaker with horn (the right of

Fig. 5e). Furthermore, our FASSEL fitted well on nonplanar surfaces, making it comparable with a variety of wearable, skin-mountable devices, as shown in Fig. 5f.

Supplementary data related to this article can be found at https://doi.org/10.1016/j.nanoen.2019.03.006.

4. Conclusion

Artificial synesthesia of simultaneously recognizing sound and vision was demonstrated in a single device platform of a flexible thin film device with sound-synchronized EL. A flexible piezoelectric polymer composite thin film with light-emitting inorganic phosphor particles successfully suited the purpose. The FASSEL made of a thin polymer composite of a piezoelectric PVDF-TrFE and field-induced light-emitting ZnS microparticles was responsive to continuous AC sound input signals. In addition to signal-dependent sound generation in the composite film arising from the piezoelectric actuation of the PVDF-TrFE, EL also occurred simultaneously due to the solid-state cathode luminescence of ZnS depending upon the AC fields, leading to a high-performance sound-synchronized EL in a single device. The effective synchronized piezoelectric sound generation and EL emission was achieved by carefully adjusting the poling field, annealing temperature, and amount of ZnS microparticles encapsulated with the controlled silica shells. By employing transparent polymer electrodes, we were able to develop a mechanically flexible, foldable, and even crumpled FASSEL whose shape can be readily altered without significant performance degradation, enabling various unconventional applications of standalone lighting speakers, origami-foldable ones and skin-mountable EL ones. Our mechanically flexible thin-film artificial synesthesia electronic device offers a human-friendly platform for realizing artificial vision–sound synesthesia and thus for developing wearable, on-body sound-interactive displays suitable not only for personal visual protection systems from sound indistinguishable environment but also for medical devices which can assist infants, babies, the elderly and hearing-impaired patients.

Notes

The authors declare no competing financial interest.

Acknowledgements

This research was supported by a grant from the National Research Foundation of Korea, funded by Korean government (MEST) (No. 2017R1A2A1A05001160, NRF-2016M3A7B4910530, 2016R1A-3B1908431, 2018M3D1A1058536) and by the third stage of the Brain Korea 21 Plus project in 2017.

Appendix A. Supplementary data

Supplementary data to this article can be found online at https://doi.org/10.1016/j.nanoen.2019.03.006.

References

[1] C. Larson, B. Peele, S. Li, S. Robinson, M. Totaro, L. Beccai, B. Mazzolai, R. Shepherd, Highly stretchable electroluminescent skin for optical signaling and tactile sensing, Science 351 (2016) 1071–1074.
[2] X.Y. Wei, X. Wang, S.Y. Kuang, L. Su, H.Y. Li, Y. Wang, C. Pan, Z.L. Wang, G. Zhu, Dynamic triboelectrification-induced electroluminescence and its use in visualized sensing, Adv. Mater. 28 (2016) 6656–6664.
[3] J. Zhong, H. Zhu, Q. Zhong, J. Dai, W. Li, S.H. Jang, Y. Yao, D. Henderson, Q. Hu, L. Hu, J. Zhou, Self-Powered human-interactive transparent nanopaper systems, ACS Nano 9 (2015) 7399–7406.
[4] S. Li, B.N. Peele, C.M. Larson, H. Zhao, R.F. Shepherd, A stretchable multicolor display and touch interface using photopatterning and transfer printing, Adv. Mater. 28 (2016) 9770.
[5] S. Gao, X. Wu, H. Ma, J. Robertson, A. Nathan, Ultrathin multifunctional graphene-PVDF layers for multidimensional touch interactivity for flexible displays, ACS Appl. Mater. Interfaces 9 (2017) 18410–18416.
[6] Y. Zhang, Y. Fang, J. Li, Q. Zhou, Y. Xiao, K. Zhang, B. Luo, J. Zhou, B. Hu, Dual-mode electronic skin with integrated tactile sensing and visualized injury warning, ACS Appl. Mater. Interfaces 9 (2017) 37493–37500.
[7] C.C. Kim, H.H. Lee, K.H. Oh, J.Y. Sun, Highly stretchable, transparent ionic touch panel, Science 353 (2016) 682–687.
[8] M. Peng, Z. Li, C. Liu, Q. Zheng, X. Shi, M. Song, Y. Zhang, S. Du, J. Zhai, Z.L. Wang, High-resolution dynamic pressure sensor array based on piezo-phototronic effect tuned photoluminescence imaging, ACS Nano 9 (2015) 3143–3150.
[9] S.H. Cho, S.W. Lee, S. Yu, H. Kim, S. Chang, D. Kang, I. Hwang, H.S. Kang, B. Jeong, E.H. Kim, S.M. Cho, K.L. Kim, H. Lee, W. Shim, C. Park, Micropatterned pyramidal ionic gels for sensing broad-range pressures with high sensitivity, ACS Appl. Mater. Interfaces 9 (2017) 10128–10135.
[10] S.W. Lee, S.H. Cho, H.S. Kang, G. Kim, J.S. Kim, B. Jeong, E.H. Kim, S. Yu, I. Hwang, H. Han, T.H. Park, S. Jung, J.K. Lee, W. Shim, C. Park, Electroluminescent pressure-sensing displays, ACS Appl. Mater. Interfaces 10 (2018) 13757–13766.
[11] S.K. Kang, R.K.J. Murphy, S.W. Hwang, S.M. Lee, D.V. Harburg, N.A. Krueger, J. Shin, P. Gamble, H. Cheng, S. Yu, Z. Liu, J.G. McCall, M. Stephen, H. Ying, J. Kim, G. Park, R.C. Webb, C.H. Lee, S. Chung, D.S. Wie, A.D. Gujar, B. Vemulapalli, A.H. Kim, K.M. Lee, J. Cheng, Y. Huang, S.H. Lee, P.V. Braun, W.Z. Ray, J.A. Rogers, Bioresorbable silicon electronic sensors for the brain, Nature 530 (2016) 71–76.
[12] E.H. Kim, S.H. Cho, J.H. Lee, B. Jeong, R.H. Kim, S. Yu, T.W. Lee, W. Shim, C. Park, Organic light emitting board for dynamic interactive display, Nat. Commun. 8 (2017) 1–8.
[13] A. Nemiroski, G.M. Whitesides, Camouflage and display for soft machines, Science 162 (2012) 2–7.
[14] M. Zhang, S. Li, Controllable liquid colour-changing lenses with microfluidic channels for vision protection, camouflage and optical filtering based on soft lithography fabrication, SpringerPlus 5 (2016) 1–10.
[15] H.H. Chou, A. Nguyen, A. Chortos, J.W.F. To, C. Lu, J. Mei, T. Kurosawa, W.G. Bae, J.B.H. Tok, Z. Bao, A chameleon-inspired stretchable electronic skin with interactive colour changing controlled by tactile sensing, Nat. Commun. 6 (2015) 1–10.
[16] C. Wang, D. Hwang, Z. Yu, K. Takei, J. Park, T. Chen, B. Ma, A. Javey, User-interactive electronic skin for instantaneous pressure visualization, Nat. Mater. 12 (2013) 899–904.
[17] C. Yu, Y. Zhang, D. Cheng, X. Li, Y. Huang, J.A. Rogers, All-elastomeric, strain-responsive thermochromic color indicators, Small 10 (2014) 1266–1271.
[18] C. Yu, Y. Li, X. Zhang, X. Huang, V. Malyarchuk, S. Wang, Y. Shi, L. Gao, Y. Su, Y. Zhang, H. Xu, R.T. Hanlon, Y. Huang, J.A. Rogers, Adaptive optoelectronic camouflage systems with designs inspired by cephalopod skins, Proc. Natl. Acad. Sci. Unit. States Am. 111 (2014) 12998–13003.
[19] S.H. Cho, J. Sung, I. Hwang, R.H. Kim, Y.S. Choi, S.S. Jo, T.W. Lee, C. Park, High performance AC electroluminescence from colloidal quantum dot hybrids, Adv. Mater. 24 (2012) 4540–4546.
[20] Y. Chen, Y. Xia, G.M. Smith, D.L. Carroll, Frequency-dependent, alternating current-driven, field-induced polymer electroluminescent devices with high power efficiency, Adv. Mater. 26 (2014) 8133–8140.
[21] F. Stauffer, K. Tybrandt, Bright stretchable alternating current electroluminescent displays based on high permittivity composites, Adv. Mater. 28 (2016) 7200–7203.
[22] S.-H. Bae, O. Kahya, B.K. Sharma, J. Kwon, H.J. Cho, B. Ozyilmaz, J.-H. Ahn, Graphene-P (VDF-TrFE) multilayer film for flexible applications, ACS Nano 7 (2013) 3130–3138.
[23] J.W. Suk, K. Kirk, Y. Hao, N.A. Hall, R.S. Ruoff, Thermoacoustic sound generation from monolayer graphene for transparent and flexible sound sources, Adv. Mater. 24 (2012) 6342–6347.
[24] W. Li, D. Torres, R. Díaz, Z. Wang, C. Wu, C. Wang, Z. Lin Wang, N. Sepúlveda, Nanogenerator-based dual-functional and self-powered thin patch loudspeaker or microphone for flexible electronics, Nat. Commun. 8 (2017) 15310.
[25] L. Xiao, Z. Chen, C. Feng, L. Liu, Z.Q. Bai, Y. Wang, L. Qian, Y. Zhang, Q. Li, K. Jiang, S. Fan, Flexible, stretchable, transparent carbon nanotube thin film loudspeakers, Nano Lett. 8 (2008) 4539–4545.
[26] Y.J. Park, S.J. Kang, B. Lotz, A. Thierry, K.J. Kim, C. Park, M. Brinkmann, Ordered ferroelectric PVDF-TrFE thin films by high throughput epitaxy for nonvolatile polymer memory ordered ferroelectric PVDF-TrFE thin films by high throughput epitaxy for nonvolatile polymer memory, Macromolecules 41 (2008) 8648–8654.
[27] S.Y. Yang, L. Qian, F. Teng, Z. Xu, X.R. Xu, Alternating-current electroluminescence from an organic heterojunction sandwiched between two amorphous SiO2 layers, J. Appl. Phys. 97 (2005) 1–4.
[28] Y. Pan, Y. Xia, H. Zhang, J. Qiu, Y. Zheng, Y. Chen, W. Huang, Recent advances in alternating current-driven organic light-emitting devices, Adv. Mater. 29 (2017) 1–14.
[29] J. Han, M.C. Freyman, E. Feigenbaum, T.Y.-J. Han, Electro-optical device with tunable transparency using colloidal core/shell nanoparticles, ACS Photonics 5 (2018) 1343–1350.
[30] Y.A. Barnakov, M.H. Yu, Z. Rosenzweig, Manipulation of the magnetic properties of magnetite-silica nanocomposite materials by controlled stober synthesis, Langmuir 21 (2005) 7524–7527.
[31] W. Park, B.K. Wagner, G. Russell, K. Yasuda, C.J. Summers, Y.R. Do, H.G. Yang, Thin SiO2 coating on ZnS phosphors for improved low-voltage cathodoluminescence properties, J. Mater. Res. 15 (2000) 2288–2291.
[32] J. Yuan, K. Kajiyoshi, H. Sasaoka, K. Nishimura, Fabrication and characterization of silica nanocoatings on ZnS phosphor particles, Nanotechnology 18 (2007) 9.

[33] J.H. Lee, B. Jeong, S.H. Cho, E.H. Kim, C. Park, Non-volatile polymer electroluminescence programmable with ferroelectric field-induced charge injection gate, Adv. Funct. Mater. 26 (2016) 5391–5399.
[34] E.D. Using, T. Minami, T. Maeno, E. Devices, M. Kawanishi, N. Miura, H, related content flat panel light-emitting sounder using thin-film EL devices with a ceramic insulating layer, Jpn. J. Appl. Phys. 29 (1990) L315.
[35] S. Lee, T. Kang, W. Lee, M.M. Afandi, J. Ryu, J. Kim, Multifunctional Device based on phosphor-piezoelectric PZT: lighting, speaking, and mechanical energy harvesting, Sci. Rep. 8 (2018) 2–8.
[36] J. Wang, C. Yan, K.J. Chee, P.S. Lee, Highly stretchable and self-deformable alternating current electroluminescent devices, Adv. Mater. 27 (2015) 2876–2882.
[37] M. He, K. Zhang, G. Chen, J. Tian, B. Su, Ionic gel paper with long-term bendable electrical robustness for use in flexible electroluminescent devices, ACS Appl. Mater. Interfaces 9 (2017) 16466–16473.
[38] M.Y. Teo, N. Kim, S. Kee, B.S. Kim, G. Kim, S. Hong, S. Jung, K. Lee, Highly stretchable and highly conductive PEDOT:PSS/Ionic liquid composite transparent electrodes for solution-processed stretchable electronics, ACS Appl. Mater. Interfaces 9 (2017) 819–826.
[39] Y. Zhang, G. Gao, H.L.H. Chan, J. Dai, Y. Wang, J. Hao, Piezo-Phototronic effect-induced dual-mode light and ultrasound emissions from ZnS:Mn/PMN-PT thin-film structures, Adv. Mater. 24 (2012) 1729–1735.
[40] S.M. Jeong, S. Song, S.K. Lee, N.Y. Ha, Color manipulation of mechanoluminescence from stress-activated composite films, Adv. Mater. 25 (2013) 6194–6200.
[41] Y. Chen, Y. Zhang, D. Karnaushenko, L. Chen, J. Hao, F. Ding, O.G. Schmidt, Addressable and color-tunable piezophotonic light-emitting stripes, Adv. Mater. 29 (2017) 1–8.
[42] S. Ummartyotin, N. Bunnak, J. Juntaro, M. Sain, H. Manuspiya, Synthesis and luminescence properties of ZnS and metal (Mn, Cu)-doped-ZnS ceramic powder, Solid State Sci. 14 (2012) 299–304.
[43] J.H. Park, S.H. Lee, J.S. Kim, A.K. Kwon, H.L. Park, S. Do Han, White-electroluminescent device with ZnS:Mn, Cu, Cl phosphor, J. Lumin. 126 (2007) 566–570.
[44] H. Teruhiko, K. Hiroji, Luminescence excitation spectra and their exciton structures of ZnS phosphors. I. Mn, (Cu, Al), and (Au, Al) doped phosphors, Jpn. J. Appl. Phys. 19 (1980) 267–277.
[45] R.N. Bhargava, D. Gallagher, Optical properties of manganese-doped nanocrystals of ZnS, Phys. Rev. Lett. 72 (1994) 416–419.
[46] H. Tian, D. Xie, Y. Yang, T.L. Ren, T.T. Feng, Y.F. Wang, C.J. Zhou, P.G. Peng, L.G. Wang, L.T. Liu, Poly(3,4-ethylenedioxythiophene):poly(styrenesulfonate)-based organic, ultrathin, and transparent sound-emitting device, Appl. Phys. Lett. 99 (2011) 2009–2012.
[47] M. Vosgueritchian, D.J. Lipomi, Z. Bao, Highly conductive and transparent PEDOT:PSS films with a fluorosurfactant for stretchable and flexible transparent electrodes, Adv. Funct. Mater. 22 (2012) 421–428.
[48] D.J. Lipomi, J.A. Lee, M. Vosgueritchian, B.C.K. Tee, J.A. Bolander, Z. Bao, Electronic properties of transparent conductive films of PEDOT:PSS on stretchable substrates, Chem. Mater. 24 (2012) 373–382.
[49] Y.F. Lin, J. Song, Y. Ding, S.Y. Lu, Z.L. Wang, Piezoelectric nanogenerator using CdS nanowires, Appl. Phys. Lett. 92 (2008) 1–4.
[50] W. Z.L, S. J, Piezoelectric nanogenerators based on zinc oxide nanowire arrays, Science 312 (2006) 242–246.
[51] T.H. Park, S. Yu, S.H. Cho, H.S. Kang, Y. Kim, M.J. Kim, H. Eoh, C. Park, B. Jeong, S.W. Lee, D.Y. Ryu, J. Huh, C. Park, Block copolymer structural color strain sensor, NPG Asia Mater. 10 (2018) 328–339.
[52] J. Ham, A.F. McGuire, J.Y. Oh, M. Krason, J. Kang, D. Son, J.W. To, Y. Liu, T. Katsumata, J.B.-H. Tok, Y. Lee, N. Matsuhisa, J. Mun, Z. Bao, U. Kraft, O. Vardoulis, Y. Kim, Y. Yun, F. Molina-Lopez, An integrated self-healable electronic skin system fabricated via dynamic reconstruction of a nanostructured conducting network, Nat. Nanotechnol. 13 (2018) 1057–1065.

Jong Sung Kim received his B.S. and M.S Degree in the Department of Chemical Engineering from Korea University. Currently, he is a Ph.D. Candidate at Materials Science and Engineering in Yonsei University and supervised by Prof. Cheolmin Park. His research interests are multi-functional interactive sensor and display based on piezoelectric, electroluminescent materials.

Sung Hwan Cho received his Ph.D. Degree in the Department of Materials Science and Engineering from Yonsei University. Currently, he is a Postdoc at Mechanical Science and Engineering of University of Illinois Urbana-Champaign (UIUC). He is working on developing flexoelectric sensor/actuator devices with 2 dimensional nanomaterials. He is also interested in developing wearable sensors and opto-electronics.

Kang Lib Kim received his B.S. Degree in the Department of Materials Science and Engineering from Yonsei University. Currently, he is a Ph.D. Candidate at Materials Science and Engineering in Yonsei University. His research interests are ferroelectric polymers and Non-volatile transistor memory.

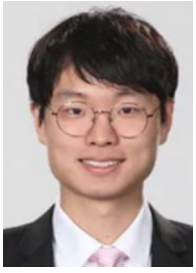

Gwangmook Kim received his B.S. Degree in the Department of Materials Science and Engineering from Yonsei University. Currently, he is a Ph.D. Candidate at Materials Science and Engineering in Yonsei University and supervised by Prof. Wooyoung Shim. His research interest is the development of instrument for high-throughput surface topography measurement.

Seung Won Lee received his B.S. degree in Material Science and Engineering from Yonsei University. He is currently a Ph.D. Candidate at Material Science and Engineering from Yonsei University under the supervision of Prof. Cheolmin Park. His research interests are luminescence materials and fabrication of multi-functional sensor & display for E-skin.

Eui Hyuk Kim received a B.S. degree in Material Science and Engineering from Yonsei University. He is currently a Ph.D. Candidate at the Department of Material Science and Engineering in Yonsei University under the supervision of Prof. Cheolmin Park. His research interests are EL materials or solution processed LEDs and multifunctional sensing display.

Beomjin Jeong received his B.S. Degree in the Department of Materials Science and Engineering from Yonsei University. Currently, he is a Ph.D. Candidate at Materials Science and Engineering in Yonsei University and supervised by Prof. Cheolmin Park. His research interests are soft lithography via polymeric materials and organic-inorganic semiconductor materials.

Ihn Hwang received his B.S., M.S. and ph.D. degree in Material Science and Engineering from Yonsei university under the supervision of Prof. Cheolmin Park. His research interests are a various electronics based on the self-assembly of organic materials. He is currently a researcher at R&D Center of LG household & health Care Co., Ltd.

Hyowon Han obtained his B.S. degree in Material Science and Engineering at Yonsei University, Korea, in 2017. He joined Prof. Cheolmin Park's group as a Ph.D. candidate in 2017. His research is mainly focused on physics and optic application of metal halide perovskites and their composites with block copolymer.

Wooyoung Shim is an assistant professor at Yonsei University in Korea. He attended the Yonsei University for his undergraduate education and graduate program for his master degree in the Department of Materials Science and Engineering. After his doctoral studies at the Northwestern University and postdoctoral research at the Harvard University, he moved back to Yonsei in 2014 to assume the position of assistant Professor. At Yonsei, he has been interested in the synthesis of a broad range of nanoscale materials and the development of methods of hierarchical assembly of nanoscale materials, together with the development of nanolithographic tools for future nanotechnology-enabled sensors and related nanoelectronics.

Tae-Woo Lee is an associate professor in the department of the materials science and engineering at Seoul National University, Korea. He received his Ph.D in chemical engineering from KAIST, Korea in February 2002. Then, he joined Bell Laboratories, USA as a postdoctoral researcher. From 2003 to 2008, he worked in Samsung Advanced Institute of Technology. From 2008 to 2016, he worked as assistant and associate professor at Pohang University of Science and Technology (POSTECH), Korea. His research focuses on organic, organic-inorganic hybrid, perovskite, and carbon & 2D materials and their applications to flexible electronics, printed electronics, displays, solid-state lightings, solar energy conversion devices, and neuromorphic devices.

Cheolmin Park is an Underwood Distinguished Professor at Yonsei University, professor of the Department of Materials Science and Engineering at Yonsei University. He received his B.S. and M.S. degree in Polymer and Fiber Engineering from Seoul National University in 1992 and 1995, respectively and a Ph.D. degree in Materials Science and Engineering from Massachusetts Institute of Technology in 2001. He was a research scientist at Korea Institute of Science and Technology. After the postdoctoral fellowship at Harvard University, he joined at Yonsei University in 2002. His research has focused on self assembled polymers and their applications to organic photoelectronics.